



# CHORUS

This is the accepted manuscript made available via CHORUS. The article has been published as:

## Identification of electronic state in perovskite $\text{CaCrO}_3$ by high-pressure studies

J.-S. Zhou, J. A. Alonso, J. Sanchez-Benitez, M. T. Fernandez-Diaz, R. Martinez-Coronado, L.-P. Cao, X. Li, L. G. Marshall, C.-Q. Jin, and J. B. Goodenough

Phys. Rev. B **92**, 144421 — Published 23 October 2015

DOI: [10.1103/PhysRevB.92.144421](https://doi.org/10.1103/PhysRevB.92.144421)

# Identification of electronic state in perovskite $\text{CaCrO}_3$ by high pressure studies

J.-S. Zhou<sup>1\*</sup>, J.A. Alonso<sup>2</sup>, J. Sanchez-Benitez<sup>3</sup>, M.T. Fernandez Diaz<sup>4</sup>, R. Martinez-Coronado<sup>2</sup>, L.-P. Cao<sup>5</sup>, X. Li<sup>1</sup>, L. Marshall<sup>1</sup>, C.-Q. Jin<sup>5</sup>, J.B. Goodenough<sup>1</sup>,

<sup>1</sup> Materials Science and Engineering program/Mechanical Engineering, University of Texas at Austin, USA

<sup>2</sup> Instituto de Ciencia de Materiales de Madrid, CSIC, Cantoblanco, E-28094 Madrid, Spain

<sup>3</sup> Departamento de Quimica Fisica, Fac.CC. Quimicas, Universidad Complutense de Madrid, E-28040 Madrid, Spain

<sup>4</sup> Institute Laue-Langevin (ILL) 156X, F-38042 Grenoble Cedex 9, France

<sup>5</sup> Institute of Physics, Chinese Academy of Sciences, Beijing 100190, China

$\text{CaCrO}_3$  is at the crossover from localized to itinerant electronic behavior, and interpretation of its electronic state has remained controversial. It is a metal from an optical study. However, the collinear type-C antiferromagnetic spin ordering below  $T_N \approx 90$  K is characteristic of localized electron magnetism. We have performed many runs of high-pressure synthesis.  $\text{CaCrO}_3$  crystals can be found in some batches. We have used specific-heat measurement as a diagnostic tool to probe the electronic states near the Fermi energy. An electronic bandwidth is broadened by applying high pressure. The magnetization measurement under pressure reveals a  $dT_N/dP < 0$ . The crystal structural change corresponding to the pressure-induced electron structural change has been monitored by *in-situ* neutron diffraction under high pressure. The  $t_2^2$  d-electron configuration on octahedral site  $\text{Cr}^{4+}$  is orbitally threefold degenerate. Local site distortions are argued to show that in  $\text{CaCrO}_3$  the crossover from localized to itinerant 3d electrons does not result in a charge-density wave in which segregation of the interatomic interactions results in the stabilization of molecular clusters, but in an intraatomic orbital ordering that stabilizes a half-filled localized-electron xy orbital and a  $1/4$ -filled c-axis  $\pi^*$  band. Local structural changes under pressure reveal a weakening of long-range magnetic order is associated with a smooth Mott-Hubbard transition of the xy electrons.

## Introduction

Mott physics is the foundation to describe strongly correlated electronic systems. However, to have a full solution of the Mott-Hubbard Hamiltonian at the crossover from localized to itinerant electronic behavior is a challenging task. Moreover, a lattice instability of the phase at crossover is high, so that the system is vulnerable to phase segregations. The crossover area can be approached experimentally in a narrow-band system by varying temperature, tuning chemical compositions, or applying high pressure. Physical properties for a system at the crossover have not been fully explored since it is always difficult to stabilize the phase in this region. We report in this paper the evolution of physical properties and crystal structure of the narrow-band perovskite  $\text{CaCrO}_3$  under high pressure.

The orthorhombic perovskite  $\text{CaCrO}_3$  was first synthesized under high pressure in the 1960s.<sup>1</sup> It is a magnetic insulator with the Neel temperature  $T_N \approx 90$  K. The magnetization measurement under pressure gave a  $dT_N/dP = -0.23$  K/kbar. Based on a semiempirical model, Goodenough *et al.* have argued that the perovskite  $\text{CaCrO}_3$  has itinerant-electron magnetism. A similar high pressure product has been obtained by Weiher *et al.*<sup>2</sup> The authors have derived a  $\mu_{\text{eff}} = 3.6 \mu_B$  and a Weiss constant  $\Theta = -920$  K by fitting the high-temperature magnetic susceptibility to 600 K to a Curie-Weiss law. The  $\mu_{\text{eff}}$  is larger than the spin only value and the absolute value of the  $\Theta$  is far beyond the expectation from the localized-electron magnetism. Their resistivity measurement on a single crystal grain indeed showed a metallic behavior over the entire temperature range except for a small resistivity jump at  $T_N$ . The metallic conductivity is consistent with the results from their magnetic susceptibility measurement, which cannot be rationalized by a localized-electron picture. Interest in a thorough understanding of the electronic state and whether a change of orbital degree of freedom is involved at  $T_N$  in  $\text{CaCrO}_3$  has been revived in recent years.<sup>3-10</sup> A neutron diffraction study has revealed in great detail the evolution of the local structural distortions as a function of temperature and the magnetic structure.<sup>5</sup> Although numerous attempts to duplicate the metallic conductivity obtained by Weiher *et al.* have all failed, the optical reflectivity on a cold-pressed powder sample showed some spectral weight at low frequency, characteristic of itinerant electron behavior.<sup>4,5</sup> However, the type-C collinear spin ordering below  $T_N$  seems troublesome for an itinerant-electron picture. Moreover, the local structure from neutron diffraction is also not compatible with the scenario of a 3D itinerant

electron state. In itinerant electron perovskites like SrVO<sub>3</sub> and CaVO<sub>3</sub>, a ratio of the M-O bond lengths along the *c* axis versus the M-O in the *ab* plane  $l_c/l_{ab} \approx 1$  holds. A  $l_c/l_{ab} < 1$  found in CaCrO<sub>3</sub> indicates that one of the two  $\pi$ -bonding electrons is ordered into an *xy* orbital. The controversy over whether the 3d electrons in CaCrO<sub>3</sub> are localized or itinerant could be resolved through a structural study under high pressure. Pressure provides a clean tuning of the bandwidth. Localized  $t_2$  electrons will be delocalized under a sufficiently high pressure so that a bond length ratio  $l_c/l_{ab} \approx 1$  should be obtained. Motivated by this idea, we performed neutron diffraction under high pressure and magnetization measurement under high pressure. The early day high-pressure study on CaCrO<sub>3</sub> was made up to 6 kbar.<sup>1</sup> While the hydrostatic pressure in the experiment was well-maintained since the pressure chamber was loaded with helium gas, the pressure range was too small for a structural study to detect reliably a corresponding structural change. In this paper, we report a high-pressure magnetization study of CaCrO<sub>3</sub> to 4 GPa with a diamond anvil cell. Since the electrical contact on the surface of CaCrO<sub>3</sub> samples has been problematic, we have explored a specific-heat measurement at low temperature to probe the electronic state near the Fermi energy without using an electrical contact.

## Experimental details

The starting materials used for synthesis were CaO and CrO<sub>2</sub>. In order to reduce impurities, 5% excess CaO was used. The materials were mixed thoroughly and then pressed into pellets. These pellets were sealed in gold capsules before being loaded into a cubic multianvil apparatus. Syntheses were performed under 6 GPa at 1000 °C for 30 min followed by **rapidly cooling** the sample before releasing the pressure. The high-pressure products were characterized with X-ray powder diffraction and SEM. Whereas all batches of samples were made under an identical pressure and temperature, large single crystals were found in some batches of the high-pressure products, see SEM pictures in Fig.1. By using rotating sample X-ray diffraction, we have studied the crystal structure of a single crystal and a small cluster of polycrystalline sample picked up from different batches. Although two Néel temperatures can be well-distinguished by specific heat measurements as will be discussed in the next section, single-crystal and polycrystalline samples show an identical XRD pattern and the same lattice parameters within the experimental uncertainty. The specific heat measurements were performed with a Physical Property Measurement System (PPMS) (Quantum Design) by using the two- $\tau$  relaxation method. The

magnetization measurements under high pressure on a single-crystal sample of  $\text{CaCrO}_3$  were performed with two devices, a Be-Cu piston-cylinder device (PCD) and a miniature diamond anvil cell (DAC) fit to a Superconductor Quantum Interference Device (SQUID) magnetometer (Quantum Design). Daphne 7373 was used as the pressure medium. The pressure was determined by measuring the superconducting transition temperature of Pb. The signal from the sample loaded in a DAC is at the limit of the SQUID in this study; but the change of  $T_N$  under pressure could still be resolved. Neutron powder diffraction (NPD) experiments under high pressure were performed at the high-flux D20 diffractometer of the Institut Laue-Langevin (ILL) in Grenoble, France. The high-resolution mode (take-off angle of  $120^\circ$ ) was selected with a wavelength  $1.866(1) \text{ \AA}$ . The sample, mixed with MgO powder as **the internal standard material for measuring the pressure**, was loaded into an encapsulated TiZr gasket filled with a 4:1 mixture of methanol-ethanol as a pressure medium before pressing in a Paris-Edinburgh (PE) device. The NPD patterns were analyzed by the Rietveld method with the FULLPROF program.

## Results

### 1. The SEM results

While we have kept the pressure and temperature identical in each run of high-pressure synthesis, shining single-crystal cubes are visible under a microscope in some batches. However, X-ray diffraction on powder obtained by crushing all high-pressure products shows a single phase of  $Pbnm$  perovskite with identical lattice parameters. Fig.1 illustrates the SEM pictures taken on three typical samples. Sample A is a uniformly polycrystalline sample. Sample B is a polycrystalline sample with a few embedded crystals. Sample C is a polycrystalline sample, but embedded crystals occupy more than 1/3 of the sample's volume. The largest crystal in sample C is about  $150 \mu\text{m}$ . Crystals from sample C were separated from their polycrystalline matrix mechanically and were used for measurements of specific heat and the magnetization under high pressure.

### 2. Specific heat results

Fig.2 shows the detail of specific heat near the transition temperature. The major features of the specific heat data include (1) a broad hump at  $\sim 82 \text{ K}$  and a sharp peak at  $89 \text{ K}$ . Sample A shows only a broad hump of  $C_p$  at  $82 \text{ K}$ . Sample B with a few embedded crystals shows two humps, a

broad one at a slightly higher temperature than 82 K and the second one at 89 K. Sample C with many embedded crystals shows essentially the same  $C_p$  as that from single crystals separated from this sample. A comparison between samples B and C indicates the crystals all have an identical higher  $T_N$  than that of their polycrystalline matrix and of the uniformly polycrystalline sample. A higher  $T_N$  and sharp transition normally corresponds to an oxygen-stoichiometric sample as well as the crystalline quality in oxides. It also means that the oxygen content distribution in the sample is not uniform at the initial stage of the sample's synthesis. The oxygen-rich regions appear to have a lower melting temperature in order to form a nucleus that grows into a single crystal during synthesis.

In the plot of  $C_p/T$  versus  $T^2$  of Fig.3, data from sample A fall along a line at low temperatures. Surprisingly, the linear fitting remains good to a relatively high temperature. A non-zero  $\gamma$  from the intercept between the fitting line and the vertical axis indicates that sample A is a metal with a non-electrical contact method. For sample B with a few embedded single crystals, two obvious changes are observed: (1) a small upturn deviation of the last few temperature points close to the lowest temperature found in sample A becomes more pronounced and (2) while the data still fall along a line to nearly the same high temperature point as in the sample A, the slope of the fitting line changes slightly and the intercept to the vertical axis decreases. These trends become even more clear in sample C. As for the crystals separated from sample C, the intercept approaches zero and the low temperature upturn can be clearly identified. It is clear that single crystal are responsible for the two features (1) and (2) in Fig.3. A low-temperature upturn in the  $C_p/T$  versus  $T^2$  plot is commonly observed in other magnetic insulators due to the residual spin fluctuations (even in magnetically ordered phases). A linear fitting in a  $C_p/T$  versus  $T^2$  plot does not normally extend to higher temperatures where the  $\beta T^3$  term is no longer a good approximation for describing the lattice contribution. By taking advantage of the observation that the  $\beta T^3$  appears to be a good approximation to a high temperature in the  $C_p$  of  $\text{CaCrO}_3$ , we can extract  $\gamma$  from a linear fitting to high temperatures. Then the conclusion is clear and consistent. Sample A is a metal with a broad transition at  $T_N \sim 82$  K. The single-crystal sample is an insulator with oxygen stoichiometry and a much sharper transition at  $T_N \sim 89$  K. A detailed analysis of the critical behavior at  $T_N$  and its interpretations in the single-crystal sample will be published separately.<sup>11</sup>

### 3. Magnetization measurements under high pressure

The temperature dependence of magnetization for  $\text{CaCrO}_3$  under high pressure was measured with a piston-cylinder device (PCD) to 10 kbar and a DAC to 50 kbar. Fig.4(a,b) show the results. The sample volume loaded in a DAC is about three orders of magnitude smaller than that used in a PCD, see the image of the DAC gasket and a chip of the sample inside in the inset of Fig.4(b). The signal from a DAC is at the limit that the SQUID magnetometer can resolve. The signal is noisy; but the magnetic transition can still be identified. Both  $T_N$  and the magnetization below  $T_N$  decrease under pressure. The pressure dependences of  $T_N$  obtained from both devices are plotted in Fig.5. A linear fitting gives a  $dT_N/dP = -0.41(4)$  K/kbar for the PCD and  $-0.48(6)$  K/kbar for the DAC. The magnitude of  $dT_N/dP$  is a factor two higher than that reported in the early study.<sup>1</sup> This discrepancy can be attributed to an oxygen non-stoichiometry of the polycrystalline sample made in the early study since the transition width of that sample looks much broader than that of the single-crystal sample in this study.

#### 4. Neutron diffraction under high pressure

Patterns of neutron diffraction on  $\text{CaCrO}_3$  and the result of refinement at two pressure points are shown in Fig.6. The hump at  $2\theta \approx 25^\circ$  in the pattern (it moves to a higher value of  $2\theta$  as pressure increases) is from the pressure medium. The quality of the refinement based on the  $Pbnm$  perovskite structural model is good and it remains unchanged at higher pressures. All parameters from the refinement are listed in Table I and the pressure dependences of bond lengths and bond angles are plotted in Fig.7. The result for the sample sealed in the PE cell (a few kbar to seal the chamber) is comparable to the result of neutron diffraction obtained at ambient pressure reported previously.<sup>5</sup> While all Cr-O bond lengths decrease under pressure, the bond length  $l_{ab}$  is more compressible than the  $l_c$ . Therefore, the  $l_c/l_{ab}$  ratio increases gradually with pressure. The ratio is also compared to that in isostructural  $\text{CaVO}_3$  and  $\text{CaTiO}_3$ .<sup>12,13</sup> The structural study on  $\text{CaTiO}_3$  was done with X-ray diffraction and the error bar size is relatively large; its  $l_c/l_{ab}$  ratio is more or less pressure independent. Nevertheless, the  $l_c/l_{ab}$  ratio in the range of 0.995 to 0.997 for  $\text{CaTiO}_3$  ( from ambient pressure to 8 GPa) and  $\text{CaVO}_3$  at ambient pressure is clearly higher than that in  $\text{CaCrO}_3$  and the pressure effect on  $\text{CaCrO}_3$  is to increase the  $l_c/l_{ab}$  ratio from 0.993 to a value comparable to that in  $\text{CaTiO}_3$  and  $\text{CaVO}_3$ . This observation is critical for us to identify the peculiar electronic state in  $\text{CaCrO}_3$ . It is also important to notice that the averaged Cr-O-Cr bond angle decreases slightly as pressure increases due to an unusual decrease of the Cr-O<sub>1</sub>-Cr bond

angle under pressure. For perovskite oxides with the geometric tolerance factor  $t < 1$ , but close to 1, the M-O-M bond angle normally increases under pressure.<sup>14-18</sup> The anomalous pressure dependence of the bond angle is related to the anisotropic bond length compressibility and the unusually large Cr-O<sub>1</sub>-Cr bond angle along the  $c$  axis in CaCrO<sub>3</sub> compared to that in other  $Pbnm$  perovskites.

## Discussions

In CaCrO<sub>3</sub>, a cooperative rotation of the CrO<sub>6</sub> octahedral sites lowers the crystal symmetry from the cubic to orthorhombic, and these site rotations induce an intrinsic site distortion to orthorhombic symmetry. The intrinsic orthorhombic site symmetry normally biases the orbital ordering that removes a threefold orbital degeneracy of a localized-electron manifold of two  $\pi$ -bonding d electrons. In CaCrO<sub>3</sub>, the cooperative orbital ordering induces a tetragonal ( $l_c/l_{ab} < 1$ ) site symmetry that competes with the intrinsic site symmetry. From a measurement of the change in the magnetic-ordering temperature versus the M-O-M d-orbital overlap in a transition metal AMO<sub>3</sub> perovskite, it is possible to distinguish a localized d-electron interatomic spin-spin interaction from that of a delocalized d-electron spin-spin interactions with a Hubbard  $U$  greater than the bandwidth  $W$ . A semi-empirical model<sup>1</sup> proposed by Goodenough *et al.* explains that  $T_N$  increases as the electron bandwidth broadens under pressure for localized-electron magnetism;  $T_N$  peaks out at the crossover from localized to itinerant behavior followed by a sharp decline as the bandwidth further broadens. Since pressure provides a clean tuning of the electron bandwidth, the empirical model can be easily transferred into a testable version, *i.e.*  $dT_N/dP > 0$  for the localized electron magnetism and  $dT_N/dP < 0$  for itinerant-electron magnetism. Furthermore, the Bloch rule  $\alpha = d\log T_N/d\log V \approx -3.3$  provides a quantitative test whether the perturbation formula of the superexchange interaction is fulfilled for localized electron magnetism.<sup>19</sup> Since the perturbation expression fails as the crossover is approached from the localized electron side, whether the  $|\alpha|$  deviates significantly from 3.3 can be used as a guide to determine the electronic state at the crossover.<sup>20</sup> Therefore, the Bloch rule is more useful than simply testing the sign of  $dT_N/dP$ . By resolving the Mott-Hubbard Hamiltonian numerically, Rozenberg *et al.* have shown the evolution of  $T_N$  versus the bandwidth covering the entire range from localized to itinerant electronic behavior.<sup>21</sup> They showed that the transition from a metallic phase to the Mott insulator phase doesn't occur at a critical on-site correlation energy  $U_c$ ; but the

localized and itinerant-electron phases are separated by a crossover area at high temperatures in the phase diagram of temperature versus  $U$ . They have also predicted that the magnetic ordering temperature changes smoothly over the entire crossing region from Mott insulator to strongly correlated metal and peaks out at the crossover. This result confirms the essential feature of the semi-empirical model by Goodenough *et al.*<sup>1</sup> A  $dT_N/dP < 0$  obtained in the early study and in this study over an even broader pressure range indicates that itinerant-electron magnetism should be operative in  $\text{CaCrO}_3$ .

On the other hand, whether electrons are localized or itinerant is also reflected in the local crystal structure. For localized electronic states, the bond valence sum (BVS) calculation based on the **nearest-neighbor** bond lengths and their coordination of the cation normally gives a valence state that is close to the formal valence value except for those double perovskites and A-site ordered perovskites that are stabilized under high pressure.<sup>22</sup> A BVS calculation using the structural data in the literature<sup>5</sup> gives a  $\text{Cr}^{4.63+}$  for  $\text{CaCrO}_3$ ; a similar valence has been obtained for the paramagnetic  $\text{SrCrO}_3$ . The **discrepancy between the BVS value and the formal valence of Cr ion indicates an itinerant electronic state in  $\text{CaCrO}_3$  since the BVS value matches the formal valence well in case of a localized electronic state.** However, an analysis of the local distortion indicates that the electron in the  $xy$  orbital is localized. In the  $Pbnm$  perovskite oxides, M-O bond lengths are split into long, medium and short bonds due to an intrinsic structural distortion.<sup>23,24</sup> However, the bond length splitting is extremely small either in transition-metal perovskites without d electrons like  $\text{CaTiO}_3$  or in perovskites with itinerant d electron like  $\text{CaVO}_3$ . The splitting is also very small in the Jahn-Teller active systems like  $\text{RTiO}_3$  and  $\text{RVO}_3$ <sup>24</sup> (R is rare earth and Y) where orbitals are disordered in the paramagnetic phase. Orbital ordering, a clear sign for localized electrons, significantly enlarges the bond length splitting by an order of magnitude and also makes the local distortion directional.<sup>24,25</sup> The bond-length splitting distortion in  $\text{CaCrO}_3$  below  $T_N$  is comparable to that in the JT active system  $\text{YVO}_3$  below an orbital ordering temperature  $T_{OO}$ .<sup>26,27</sup> This observation places  $\text{CaCrO}_3$  on the localized-electron side. The  $xy$  orbital occupation expands the  $ab$  planes. On the other hand, a close look into the local bond length indicates the  $l_c = 1.900 \text{ \AA}$  of the Cr-O bond length along the  $c$  axis is shorter than  $l_c = 1.906 \text{ \AA}$  in  $\text{SrCrO}_3$ ,<sup>5</sup> which indicates that the  $yz \pm izx$  electron is delocalized along the  $c$  axis. An easy magnetic axis on the  $b$  axis found from neutron diffraction further confirms that the possible orbital angular momentum associated with  $yz \pm izx$  is fully quenched, which in turn

supports itinerant electrons along the  $c$  axis. A longer  $l_{ab} = 1.910 \text{ \AA}$  of the Cr-O bond in the basal plane indicates that the  $xy$  electron is localized. The  $1/4$ -filled  $\pi^*$  band along the  $c$  axis gives a ferromagnetic coupling between antiferromagnetic interaction in the basal plane through localized  $xy$  electrons. The peculiar electronic configuration makes the bond length ratio  $l_c/l_{ab} < 1$ , which cannot be found in metallic perovskites or in perovskite insulators with disordered orbitals. The metallic Cr-O<sub>1</sub> bond along the  $c$  axis is less compressible than the Cr-O<sub>2</sub> bonds of the  $ab$  plane, which explains why the Cr-O<sub>1</sub>-Cr bond angle decreases under pressure. The change of the  $l_c/l_{ab}$  ratio under pressure shown in Fig.7 indicates that high pressure destroys the magnetic phase by gradually delocalizing the  $xy$  electron, *i.e* by shifting the  $l_c/l_{ab}$  ratio back to the level seen in itinerant electron CaVO<sub>3</sub>. It is because the Cr-O bond length in CaCrO<sub>3</sub> is at the crossover from itinerant to localized 3d electrons that an increase in the bond lengths in the basal plane and a decrease in the bond length along the  $c$  axis can stabilize a more localized electron in the  $xy$  orbital and an itinerant electron in a  $c$ -axis  $\pi^*$  band to quench the intraatomic spin-orbit coupling of the  $yz \pm izx$  electrons. Although a  $dT_N/dP < 0$  has been observed upon applying pressure, a metallic CaCrO<sub>3</sub> near room temperature can only be obtained under  $P > 30 \text{ GPa}$  to close the energy gap  $U > W$ .<sup>28</sup> One may question why a  $1/4$ -filled  $\pi^*$  band along the  $c$  axis does not give a metallic behavior in the single crystal CaCrO<sub>3</sub> under ambient condition. We speculate that a weak structural modulation along the  $c$  axis opens up a band gap at the Brillouin boundary on the direction. By extrapolating the  $T_N$  versus pressure curve to zero Kelvin in Fig.8 **in which the result of the transport property under pressure obtained previously is also superimposed**, we find the interesting outcome that CaCrO<sub>3</sub> would remain an insulator at the pressure where  $T_N$  vanishes. This means that CaCrO<sub>3</sub> undergoes a transition from a Mott insulator to a band insulator before finally becoming a metal as pressure increases.

## Conclusion

The 3d electrons of an oxygen-stoichiometric CaCrO<sub>3</sub> single crystal are at the crossover from localized to itinerant electronic behavior. Instead of stabilizing a charge-density wave by the segregation into molecular-orbital clusters, a local structural distortion segregates itinerant and localized electrons on a Cr cation by orbital ordering. The orbital ordering stabilizes an itinerant  $yz \pm izx$  electron in a  $1/4$ -filled  $c$ -axis  $\pi^*$  band and a localized electron in a half-filled  $xy$  orbital that gives antiferromagnetic coupling in the  $ab$  plane. Ferromagnetic coupling along the  $c$  axis

and antiferromagnetic coupling in the  $ab$  plane are responsible for type-C spin ordering found below  $T_N$  in  $\text{CaCrO}_3$ . The structural study under high pressure leads to a microscopic interpretation of a  $dT_N/dP < 0$  from the magnetization measurement. Instead of signaling that all the 3d electrons are responsible for an itinerant-electron antiferromagnetism, it is the result of a transformation of the  $xy$  electron from localized to itinerant behavior in the presence of an itinerant ( $yz \pm i zx$ ) electron. We have also identified a transition under pressure to a band insulator before it becomes a metal.

### Acknowledgment

This work was supported by the National Science Foundation (DMR MIRT 1122603) and Robert A Welch Foundation (F-1066) in the US. JAA, RMC, JSB, and MTF thank the Spanish MINECO project MAT2013-41099-R and RyC-2010-06276 for financial support.

\*jszhou@mail.utexas.edu

### References

1. J.B. Goodenough, J.M. Longo, and J.A. Kafalas, Mater. Res. Bull. **3**,471 (1968)
2. J.F. Weiher, B.L. Chamberland, and J.L. Gillson, J. Solid State Chem. **3**, 529 (1971)
3. J.-S. Zhou, C.-Q. Jin, Y.-W. Long, L.-X. Yang, and J.B. Goodenough, Phys. Rev. Lett. **96**, 046408 (2006)
4. A.C. Komarek, S.V. Streltsov, M. Isobe, T. Moller, M. Hoelzel, A. Senyshyn, D. Trots, M.T. Fernandez-Diaz, T. Hansen, H. Gotou, T. Tagi, Y. Ueda, V.I. Anisimov, M. Gruniger, D.I. Khomskii, and M. Braden. Phys. Rev. Lett. **101**, 167204 (2008)
5. A.C. Komarek, T. Moller, M. Isobe, Y. Drees, H. Ulbrich, M. Azuma, M.T. Fernandez-Diaz, A. Senyshyn, M. Hoelzel, G. Andre, Y. Ueda, M. Gruniger, and M. Braden, Phys. Rev. B **84**, 125114 (2011)
6. S.V. Streltsov, M.A. Korotin, V.I. Anisimov, and D.I. Khomskii, Phys. Rev. B **78**, 54425 (2008)
7. P.A. Bhobe, A. Chainani, M. Taguchi, R. Eguchi, M. Matsunami, T. Ohtsuki, K. Ishizaka, M. Okawa, M. Oura, Y. Senda, H. Ohashi, M. Isobe, Y. Ueda, and S. Shin, Phys. Rev. B **83**, 165132 (2011)
8. H.-M. Liu, C. Zhu, C.-Y. Ma, S. Dong, J.-M. Liu, J. Appl. Phys. **110**, 73701 (2011)
9. O. Ofer, J. Sugiyama, M. Mansson, K.H. Chow, E.J. Ansaldo, J.H. Brewer, M. Isobe, Y. Ueda, Phys. Rev. B. **81**, 184405 (2010)

10. E. Castrillo-Martinez, A. Duran, and M.A. Alario-Franco, J. Solid State Chem. 181, 895 (2008)
11. J.-S. Zhou, unpublished.
12. J. Zhao, N.L. Ross, D. Wang, and R.J. Angel, J. Phys. Condens. Matter **23**, 455401 (2011)
13. H. Falcon, J.A. Alonso, M.T. Casais, M.J. Martinez-Lope, and J. Sanchez-Benitez, J. Solid State Chem. **177**, 3099 (2004)
14. J.-S. Zhou, J.A. Alonso, A. Munoz, M.T. Fernandez-Diaz, and J.B. Goodenough, Phys. Rev. Lett. 106, 57201 (2011)
15. J. Zhao, N.L. Ross, and R.J. Angel, Acta Crystallographica B 60, 263 (2004)
16. N.L. Ross, J. Zhao, and R.J. Angel, J. Solid State Chem. 177, 1276 (2004)
17. N.L. Ross, J. Zhao, and R.J. Angel, J. Solid State Chem. 177, 3768 (2004)
18. R.J. Angel, J. Zhao, N.L. Ross, C.V. Jakeways, S.A.T. Redfern, M. Berkowski, J. Solid State Chem. 180, 3408 (2007)
19. D. Bloch, J. Phys. Chem. Solids, 27, 881 (1966)
20. J.-S. Zhou and J.B. Goodenough, Phys. Rev. Lett. 89, 87201 (2002)
21. M.J. Rozenberg, G. Kotliar, and X.Y. Zhang, Phys. Rev. B **15**, 10181 (1994)
22. See for example and the references therein. S.A. Larregola, J.-S. Zhou, J.A. Alonso, V. Pomjakushin, and J.B. Goodenough, Inorg. Chem. 53, 4281 (2014)
23. J.-S. Zhou and J.B. Goodenough, Phys. Rev. Lett. 94, 65501 (2005)
24. J.-S. Zhou and J.B. Goodenough, Phys. Rev. B 77, 132104 (2008)
25. J.-S. Zhou and J.B. Goodenough, Phys. Rev. B 69, 153105 (2004)
26. G.R. Blake, T.T.M. Palstra, Y. Ren, A.A. Nugroho, and A.A. Menovsky, Phys. Rev. B. 65, 174112 (2002)
27. M. Reehuis, C. Ulrich, P. Pattison, B. Ouladdiaf, M.C. Rheinstadter, M. Ohl, L.P. Regnault, M. Miyasaka, Y. Tokura, and B. Keimer, Phys. Rev. B 73, 94440 (2006)
28. L.X. Yang, Y.W. Long, C.Q. Jin, R.C. Yu, J.S. Zhou, J.B. Goodenough, H.Z. Liu, G.Y. Shen, and H.K. Mao, J. Phys. Conf. Seri. 121, 022017 (2008)

Table I The refinement results of neutron diffraction on CaCrO<sub>3</sub> at different pressures with the *Pbnm* space group.

<i>MgO</i>	<i>0 GPa</i>	<i>18.3 kbar</i>	<i>31.1 kbar</i>	<i>48.8 kbar</i>	<i>57.0 kbar</i>	<i>63.5 kbar</i>	<i>76.1 kbar</i>
<i>a</i> (Å)	5.2943(4)	5.2814(5)	5.2654(5)	5.2486(5)	5.2412(5)	5.2332(5)	5.2270(5)
<i>b</i> (Å)	5.3223(5)	5.3095(6)	5.2911(5)	5.2723(5)	5.2643(5)	5.2567(5)	5.2498(5)
<i>c</i> (Å)	7.4944(5)	7.4774(7)	7.4554(6)	7.4326(7)	7.4234(7)	7.4128(7)	7.4037(7)
<i>V</i> (Å <sup>3</sup> )	211.18(3)	209.68(4)	207.71(3)	206.08(3)	205.32(4)	204.22(4)	203.56(3)
<i>Ca</i> ( <i>x,y,I/4</i> )							
<i>x</i>	1.000(7)	1.001(6)	0.9943(3)	0.9955(3)	0.9956(4)	0.9935(2)	0.9979(2)
<i>y</i>	0.03070(1)	0.02867(2)	0.03000(1)	0.03136(3)	0.03196(2)	0.03194(2)	0.03025(2)
<i>B</i> <sub>iso</sub>	1.33(3)	1.45(7)	1.37(5)	1.41(7)	1.36(1)	1.41(2)	1.28(3)
<i>f</i> <sub>occ</sub>	1.000	1.000	1.000	1.000	1.000	1.000	1.000
<i>Cr</i> (1/2,0,0)							

$B_{iso}$	0.77(5)	0.59(4)	0.74(3)	0.72(3)	0.84(3)	0.85(1)	0.60(1)
$f_{occ}$	1.000	1.000	1.000	1.000	1.000	1.000	1.000
<b>O1 (x,y,1/4)</b>							
$x$	0.0581(3)	0.0535(2)	0.0566(2)	0.0604(2)	0.0619(3)	0.0642(2)	0.0634(2)
$y$	0.4905(3)	0.4928(3)	0.4929(2)	0.4920(2)	0.4913(2)	0.4918(3)	0.4911(2)
$B_{iso}$	1.51(1)	1.27(2)	1.19(1)	1.16(1)	1.13(1)	1.15(2)	1.05(1)
$f_{occ}$	1.000	1.000	1.000	1.000	1.000	1.000	1.000
<b>O2 (x,y,z)</b>							
$x$	0.7145(2)	0.7083(2)	0.7097(1)	0.7107(1)	0.7109(1)	0.7105(1)	0.7107(1)
$y$	0.2855(3)	0.2864(3)	0.28631(2)	0.2879(2)	0.2881(3)	0.2881(2)	0.2883(2)
$z$	0.03234(7)	0.03339(9)	0.03313(8)	0.03247(9)	0.03191(8)	0.03111(8)	0.03079(7)
$B_{iso}$	1.49(2)	1.29(4)	1.42(2)	1.23(3)	1.18(2)	1.17(2)	1.06(1)
$f_{occ}$	1.000	1.000	1.000	1.000	1.000	1.000	1.000
<b>Reliability factors</b>							
$\chi^2$	1.64	1.72	1.76	2.23	1.97	1.95	1.01
$R_p$ (%)	0.742	1.02	0.964	0.948	0.941	0.979	0.785
$R_{wp}$ (%)	1.01	1.29	1.23	1.21	1.19	1.26	1.01
$R_{exp}$ (%)	0.79	0.98	0.92	0.81	0.85	0.90	1.01
$R_{Bragg}$ (%)	7.93	5.81	5.93	7.43	7.21	6.79	6.25
<b>Distances</b>							
(Ca-O1)	2.8916	2.8596	2.8604	2.8637	2.8673	2.8627	2.8506
	2.4665	2.4795	2.4715	2.4527	2.4429	2.4462	2.4440
	2.9625	2.9374	2.9077	2.9251	2.9305	2.9268	2.9421
	2.3493	2.3580	2.3725	2.3401	2.3284	2.3236	2.3013
<Ca-O1>	<b>2.6674</b>	<b>2.6586</b>	<b>2.6530</b>	<b>2.6454</b>	<b>2.6422</b>	<b>2.6398</b>	<b>2.6345</b>
(Ca-O2)x2	2.6050	2.6228	2.5880	2.5840	2.5821	2.5771	2.5936
$x_2$	2.5928	2.5790	2.5861	2.5674	2.5590	2.5547	2.5426
$x_2$	2.3780	2.3464	2.3306	2.3310	2.3327	2.3273	2.3314
$x_2$	3.0973	3.1065	3.1120	3.1016	3.0959	3.0935	3.0721
<Ca-O2>	<b>2.6682</b>	<b>2.6636</b>	<b>2.6541</b>	<b>2.6460</b>	<b>2.6424</b>	<b>2.6381</b>	<b>2.6349</b>
(Cr-O1)	1.8964	1.8914	1.8880	1.8855	1.8846	1.8839	1.8810
(Cr-O2)x2	1.9096	1.9027	1.8960	1.8937	1.8919	1.8874	1.8861
(Cr-O2)x2	1.9114	1.9088	1.9049	1.9010	1.8962	1.8941	1.8902
<Cr-O2>	<b>1.9105</b>	<b>1.9057</b>	<b>1.9005</b>	<b>1.8973</b>	<b>1.8940</b>	<b>1.8907</b>	<b>1.8881</b>
<b>Angles</b>							
(Cr-O1-Cr)	162.94(7)	162.51(7)	161.67(2)	160.47(2)	159.96(2)	159.78(2)	159.48(3)
(Cr-O2-Cr)	156.54(2)	156.8(3)	157.12(3)	157.20(3)	157.34(3)	157.51(3)	157.58(3)

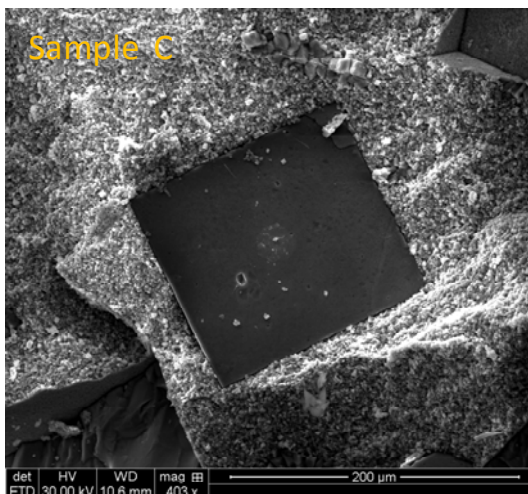
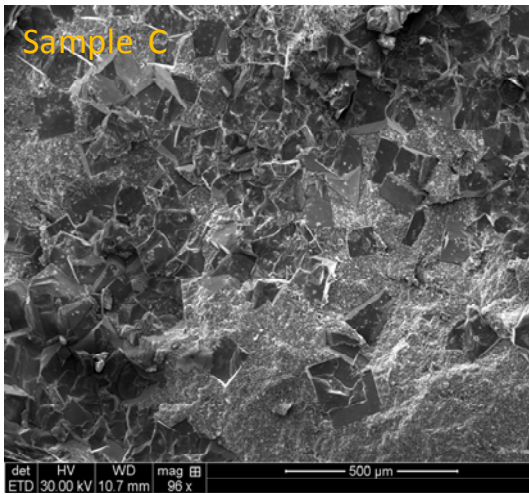
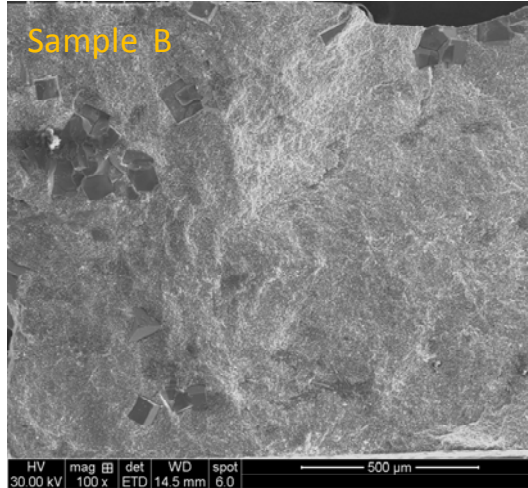
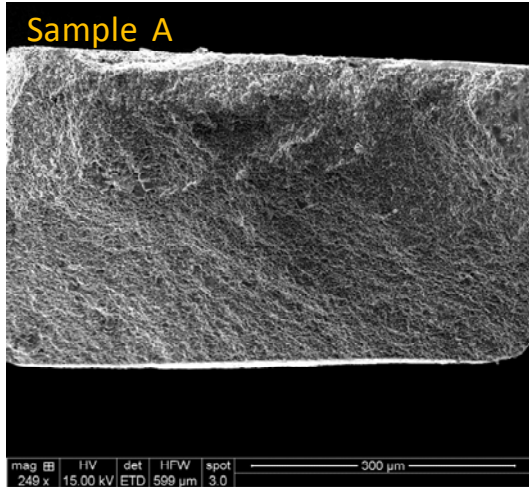


Fig. 1 The SEM picture taken on CaCrO<sub>3</sub> samples from different batches of high pressure synthesis.

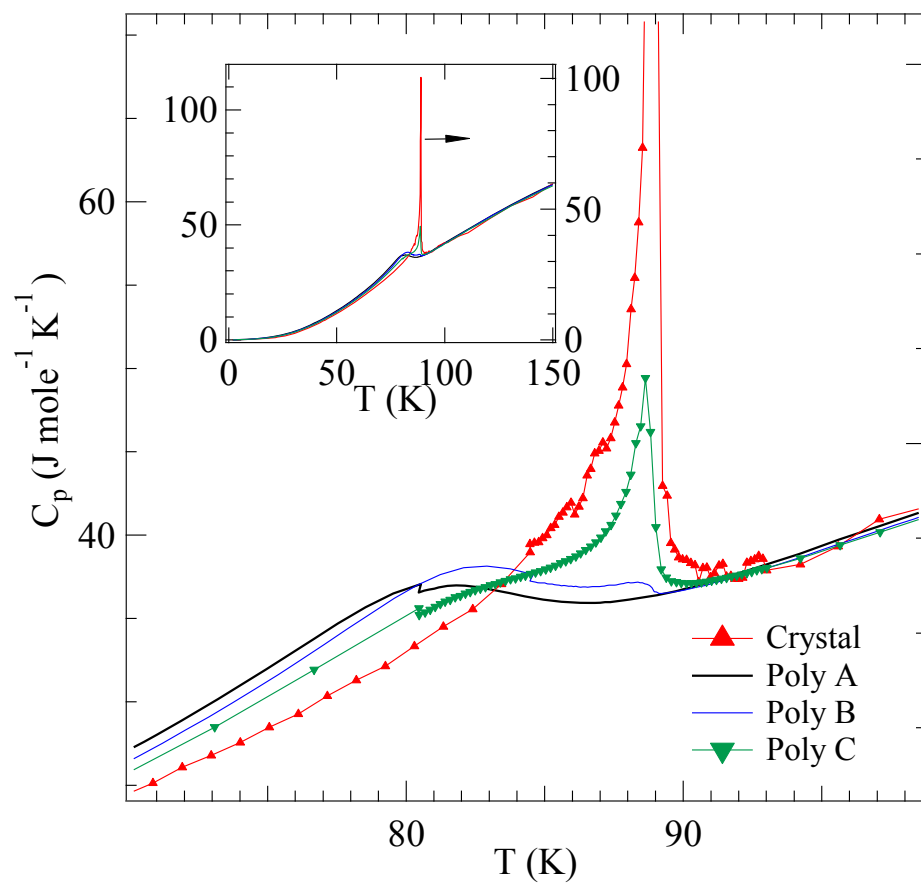


Fig.2 (Color online) Temperature dependence of specific-heat data for polycrystalline and single crystal samples of  $\text{CaCrO}_3$ .

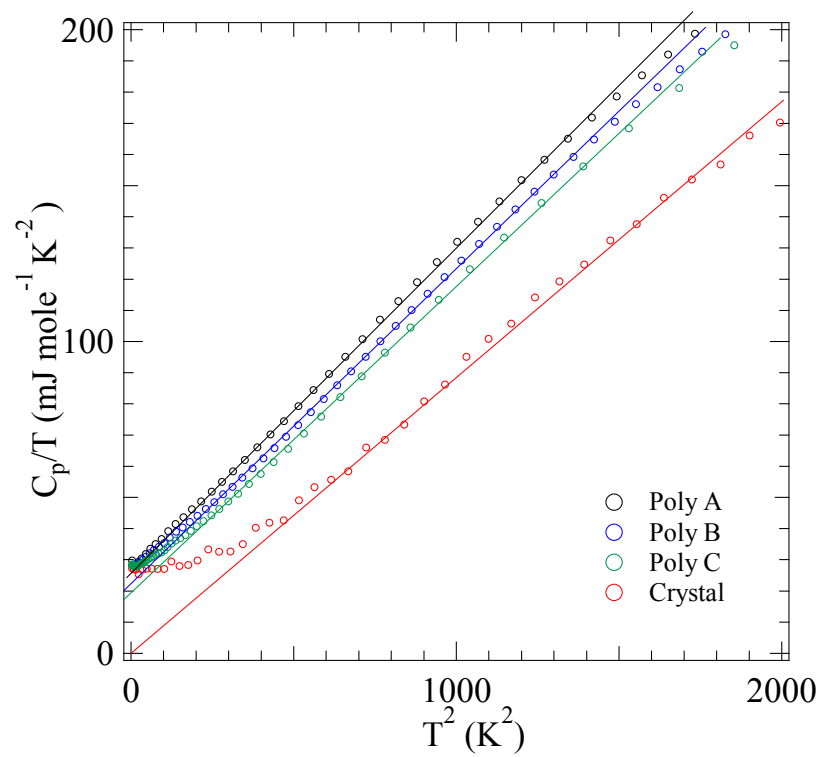


Fig. 3 (Color online) The specific-heat data in the plot of  $C_p/T$  versus  $T^2$  for polycrystalline and single crystal samples of  $\text{CaCrO}_3$ .

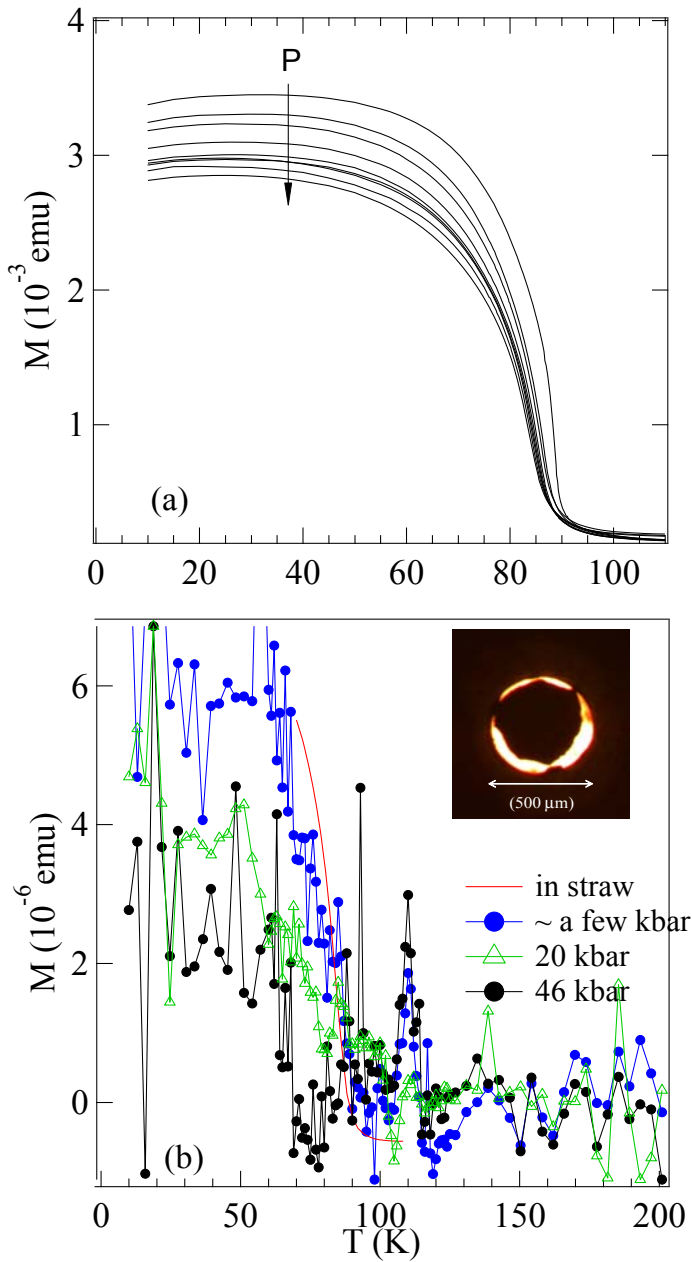


Fig.4 (Color online) Temperature dependence of the magnetization for  $\text{CaCrO}_3$  under different pressures; (a) from the piston-cylinder device, (b) from a DAC. Inset: the image of the gasket with the sample.

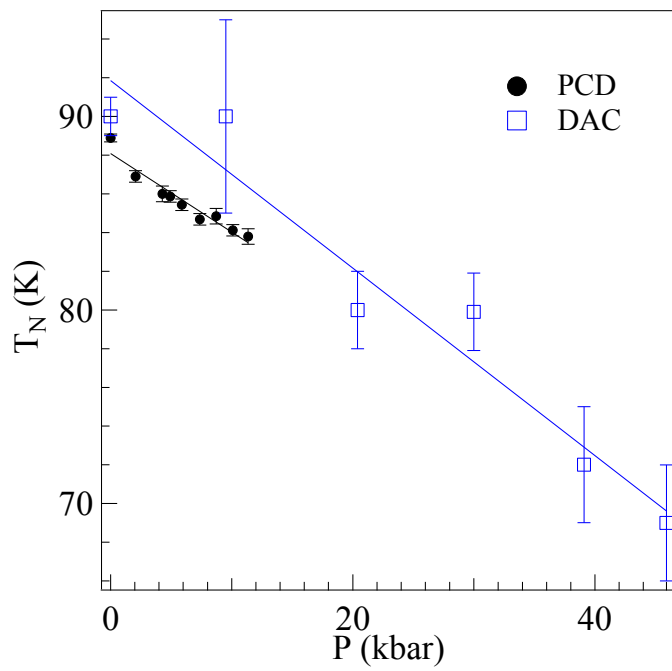


Fig. 5 (Color online) Pressure dependence of Néel temperature of  $\text{CaCrO}_3$  obtained with the piston-cylinder device (PCD) and a DAC.

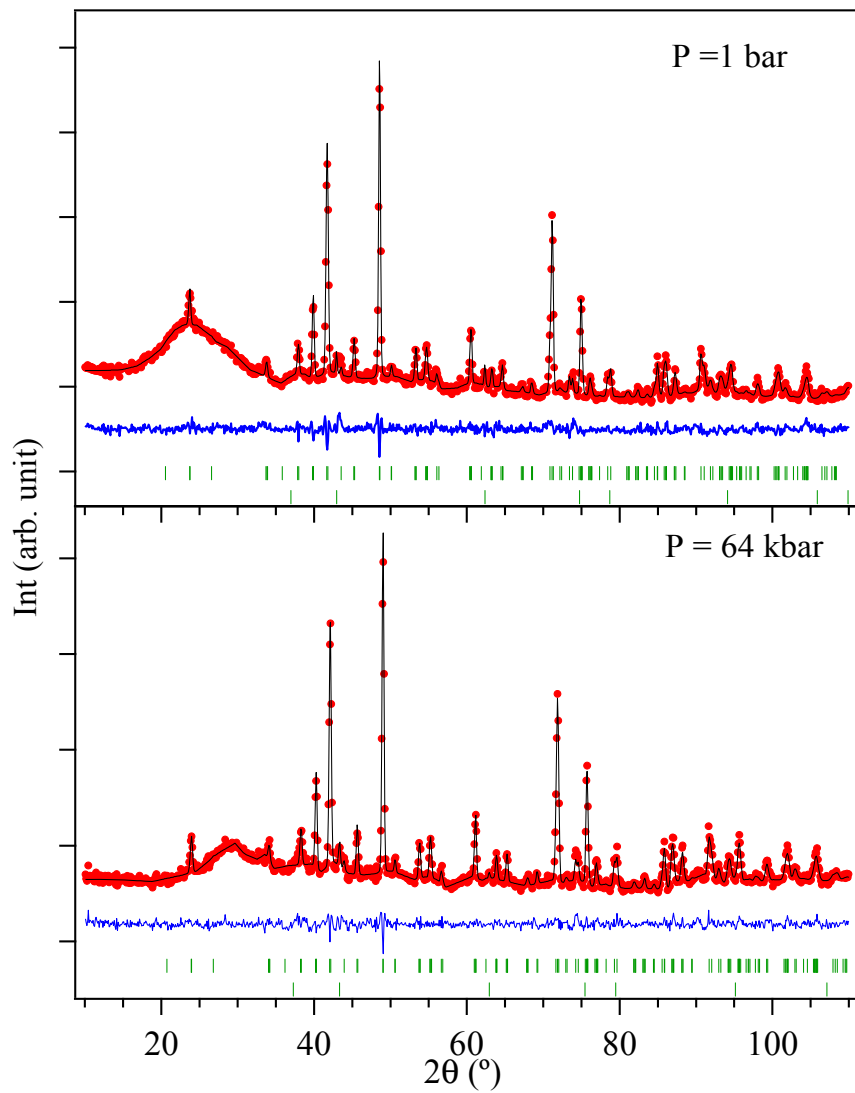


Fig. 6 (Color online) Neutron diffraction patterns and the results of refinements for  $\text{CaCrO}_3$  under two pressures; they are typical for patterns and refinements under other pressures in this work. The second row of peak position is for MgO as the internal pressure manometer.

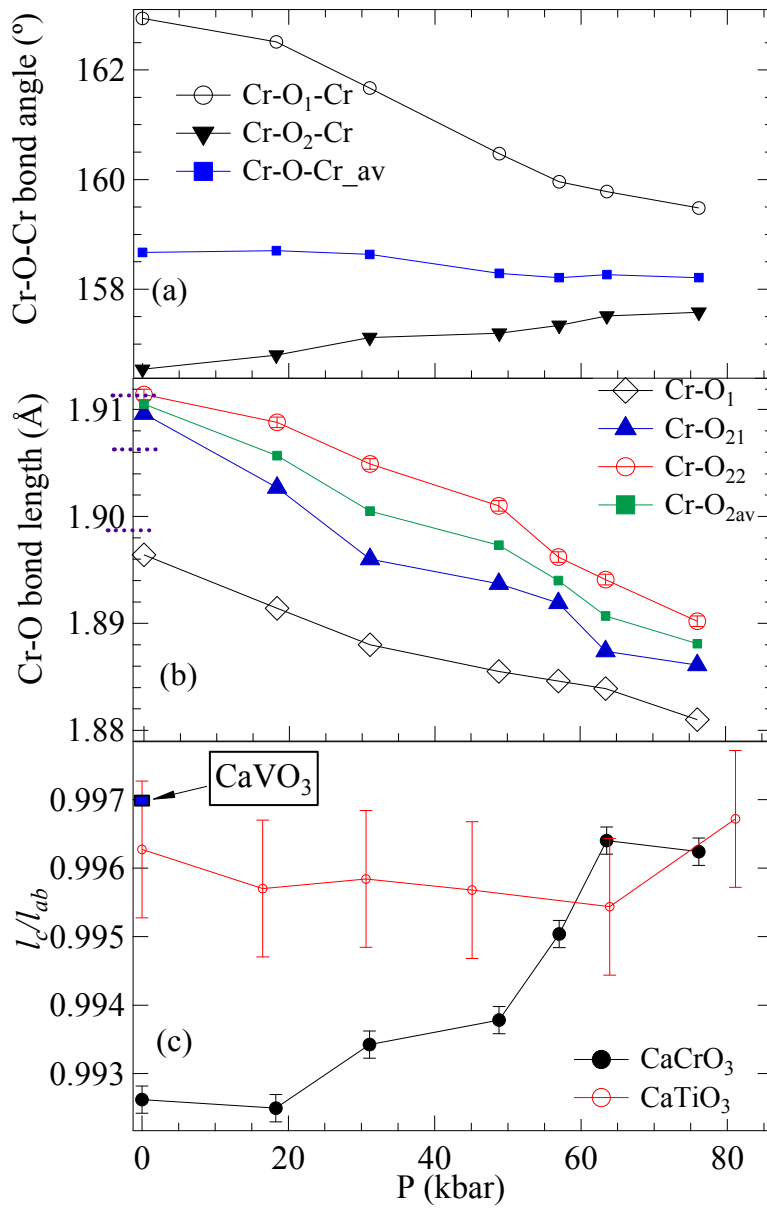


Fig.7 (Color online) Pressure dependences of (a) the bond angles, (b) bond lengths, and (c) the bond length ratio for  $\text{CaCrO}_3$ . The dashed lines in (b) indicate the Cr-O bond lengths from previous neutron study in ref.5.

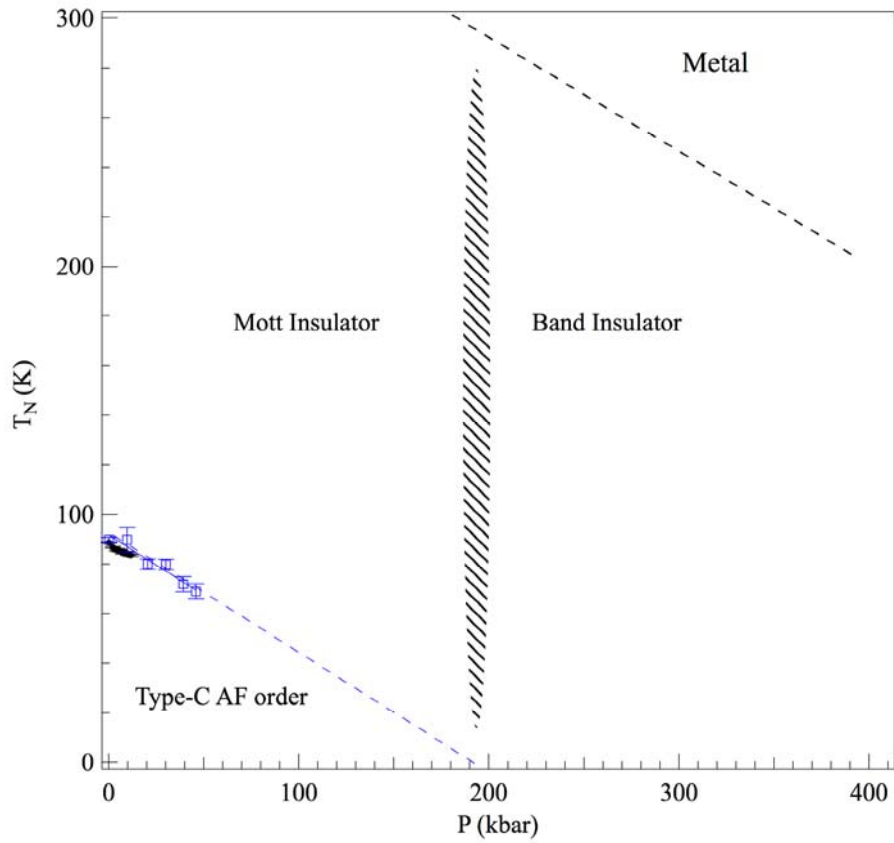


Fig.8 A projected phase diagram of  $\text{CaCrO}_3$ .